frontiers in Materials

ORIGINAL RESEARCH
published: 25 August 2020
doi: 10.3389/fmats.2020.00291

Microstructure and Properties of Ti80 Alloy Fabricated by Hydrogen-Assisted Blended Elemental Powder Metallurgy

Baicheng Wang[1], Peng Lei[1], Guangyu Ma[1], Dongdong Li[1], Dmytro Savvakin[1,2,3] and Orest Ivasishin[1,2,3]*

[1] College of Materials Science and Engineering, Jilin University, Changchun, China, [2] International Center of Future Science, Jilin University, Changchun, China, [3] G. V. Kurdyumov Institute for Metal Physics, Kyiv, Ukraine

Ti80 (Ti-6Al-3Nb-2Zr-1Mo) is a recently developed near-α titanium alloy that is generally applied in marine applications. In this study, the feasibility of producing the Ti80 alloy via the blended elemental powder metallurgy (BEPM) press-and-sinter method was demonstrated. Generally, the presence of elements with low diffusion mobility in titanium (Mo, Nb) creates difficulties with diffusion-controlled healing of the porosity and the realization of microstructural uniformity. These issues were minimized by using titanium hydride powder instead of titanium powder to activate the sintering, as well as by the proper selection of complex alloying powders rather than elemental powders to promote alloy uniformity. The sintering time-temperature conditions to obtain a chemically and microstructurally homogeneous and nearly-dense alloy microstructure were determined. Special attention was given to the microstructural peculiarities of the sintered material to regulate its mechanical characteristics. Finally, the processing parameters were determined to reach the properties required by alloy specifications. This enabled both the fully beta transformed lamellar microstructure inherent to beta phase field sintering and one that could be modified via post sintering thermomechanical processing.

Keywords: Ti80, powder metallurgy, sintering, microstructure, mechanical properties

OPEN ACCESS

Edited by:
Chao Yang,
South China University of Technology, China

Reviewed by:
Jianan Hu,
Sente Software Ltd., United Kingdom
Chenglin Li,
Wuhan University, China

****Correspondence:***
Baicheng Wang
b.c.wang@foxmail.com

Specialty section:
This article was submitted to Mechanics of Materials, a section of the journal Frontiers in Materials

Received: *19 June 2020*
Accepted: *03 August 2020*
Published: *25 August 2020*

Citation:
Wang B, Lei P, Ma G, Li D, Savvakin D and Ivasishin O (2020) Microstructure and Properties of Ti80 Alloy Fabricated by Hydrogen-Assisted Blended Elemental Powder Metallurgy. Front. Mater. 7:291. doi: 10.3389/fmats.2020.00291

INTRODUCTION

The development of materials and corresponding manufacturing technologies for marine and aerospace applications has attracted growing attention. Titanium alloys are widely used in notable applications because of their good corrosion resistance, high strength to weight ratio, and other well balanced mechanical characteristics. One of the titanium alloys used for marine application is Ti80 (Ti-6Al-3Nb-2Zr-1Mo, mass%), a new alloy developed in China, which shows a good combination of strength and weldability characteristics (Huang et al., 2011).

However, titanium products manufactured with traditional ingot metallurgy processing are generally at least 20 times more expensive than carbon steels and ∼4–5 times more expensive than stainless steels (Fang et al., 2017). The increased cost of titanium ingot metallurgy products is a result of the complicated processing required, which includes multi step vacuum remelting, hot deformation, and, finally, machining with significant material waste.

In contrast, powder metallurgy enables significant cost reduction because expensive operation steps such as vacuum remelting can be avoided and because of near net shape manufacturing of the

titanium alloy products. At the same time, powder technologies have issues related to protecting the material from impurities, which could degrade the mechanical properties. The high reactivity of titanium with oxygen, nitrogen, and carbon requires significant efforts to protect the titanium powder with a high specific surface area. Furthermore, chlorine impurities are inevitably present in titanium sponge and powders because of the Kroll manufacturing process; they remain in powder metallurgy materials in the absence of melting operations during processing, resulting in compromised mechanical properties.

A particularly low cost but effective method to achieve titanium alloys with sufficient performance is the blended elemental powder metallurgy (BEPM) method, which includes compaction and vacuum sintering of powder blends comprising the titanium base powder and master alloys (Ivasishin et al., 2000). For BEPM, using titanium hydride TiH_2 powder to replace Ti powder is beneficial in some ways. Titanium hydride is a brittle low strength material and a fine powder of the desired size can be obtained more easily than for ductile titanium. During vacuum sintering, dehydrogenation of the material with a $TiH_2 \rightarrow Ti + 2H$ phase transformation takes place, creating lots of defects in the titanium crystal lattice. This allows for accelerated diffusion, which is beneficial for improved sintering and better homogenization of the powder blends (Cao et al., 2017; Chen et al., 2017; Paramore et al., 2017). Reports have also shown that hydrogen dissolved in the crystal lattices of various metals, including titanium, promotes faster diffusion (Fukai, 2003). Furthermore, highly active atomic hydrogen emitted from the titanium crystal lattice is able to reduce surface oxides via the following reaction:

$$TiO_2 + 2H \rightarrow Ti + H_2O$$

Hydrogen also reacts with C and Cl impurities, thus, cleaning the material and provides an acceptable impurity (O, Cl, C) content in the sintered products. Finally, hydrogen is removed from the material after providing its beneficial effects during sintering and alloy formation; hence, the mechanical properties of the produced alloy are not negatively affected by the presence of hydrogen.

Previous work by Ivasishin (Ivasishin et al., 2000; Ivasishin et al., 2008; Ivasishin et al., 2012; Ivasishin and Moxson, 2015) reported various titanium alloy materials with good mechanical characteristics can be manufactured using the press-and-sinter BEPM approach with TiH_2-based powder blends. Each individual alloy composition needs careful optimization of the starting powders, including the size and chemical composition of alloying powders, compaction parameters, and time-temperature sintering regimes to achieve a desirable alloy microstructure, which is responsible for a good balance of mechanical characteristics. Earlier work on Ti80 dedicated to the influence of alloying element addition on material performance was carried out by Huang et al. (2011). This notable study demonstrated that the alloy could be produced via powder metallurgy, but failed to obtain adequate mechanical properties using TiH_2 powder, especially for elongation. This negative result could be because of the selected processing parameters, which resulted in a suboptimal microstructure and impurity content in the produced Ti80 alloy.

Given the advantages of TiH_2 powder over Ti powder for the BEPM approach, the main challenge in this work was to achieve sufficient mechanical properties for the Ti80 alloy using TiH_2 -based powder blends as a starting material. The Ti80 alloy contains elements with a low diffusion mobility in titanium (Mo, Nb). The presence of elements with a low mobility creates difficulties with diffusion-controlled healing of the porosity and achieving microstructural uniformity during BEPM fabrication (Liu et al., 2006). The present investigation was aimed at realizing a desirable microstructure and acceptable impurity content, and, hence, lead to the production of a Ti80 alloy with good mechanical properties.

MATERIALS AND METHODS

Powder Preparations

Titanium sponge from BaoTi HuaShen Titanium Industry Co., Ltd. (**Table 1**) and casted bulk 50%Al-25%Nb-16.7%Zr-8.3%Mo (mass.%) master alloy were used as starting materials in the present investigation to produce the Ti80 alloy.

Titanium sponge was hydrogenated under laboratory conditions using the prescribed heat treatment under a hydrogen atmosphere (Ivasishin and Moxson, 2015). The produced titanium hydride sponge and bulk master alloy ingot were crushed into smaller pieces; then, they were individually treated via ball milling in the planetary ball mill device to produce powders of the desired sizes. TiH_2 (∼0–65 μm) and master alloy (∼0–45 μm) powder size fractions were sieved and selected for the experiments. The selected powders were blended under an Ar atmosphere for 4 h. The morphology of the initial powders is shown in **Figure 1**.

A malvern 3000 Laser analyzer was used to investigate the size distribution of the initial powders. The size distribution of the sieved powders obeyed a Gaussian distribution, as shown in **Figure 2**, and both curves show Dx (50) in the proper section.

Consolidation of Ti-6Al-3Nb-2Zr-1Mo

The powder blends were compacted at room temperature via die pressing at 600 MPa. For this, 25 g was used for each sample to produce green compacts with a rectangular shape (65 mm in length, 10 mm in wide, and 11.25 ± 0.10 mm in height), which is convenient for further machining and tensile testing.

Various temperatures (1100, 1150,1200, 1250°C) were tested for sintering the powder compacts. The green compacts were heated in vacuum (10^{-3}Pa) with a rate of 10°C/min up to the selected temperature. Sintering duration of 3 and 4 h was chosen following our previous experience, such duration is usually enough to achieve microstructure homogeneity and sufficient

TABLE 1 | Chemical composition of the used titanium sponge.

Ti	Si	Fe	Cl	C	N	O	Mn	Mg	H
99.7	0.005	0.019	0.038	0.010	0.003	0.047	0.008	0.003	0.001

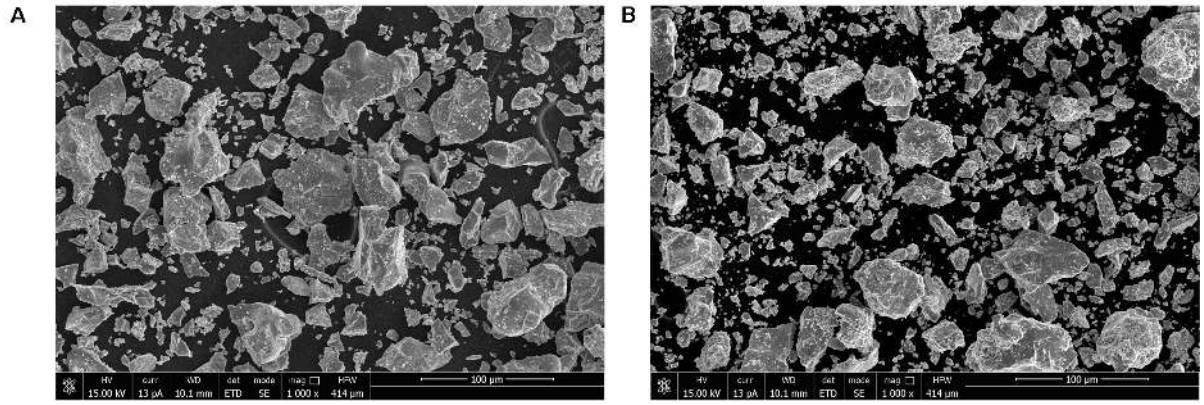

FIGURE 1 | SEM pictures showing the morphology of the starting powders of the selected sizes: **(A)** TiH2 and **(B)** 50%Al-25%Nb-16.7%Zr-8.3%Mo master alloy.

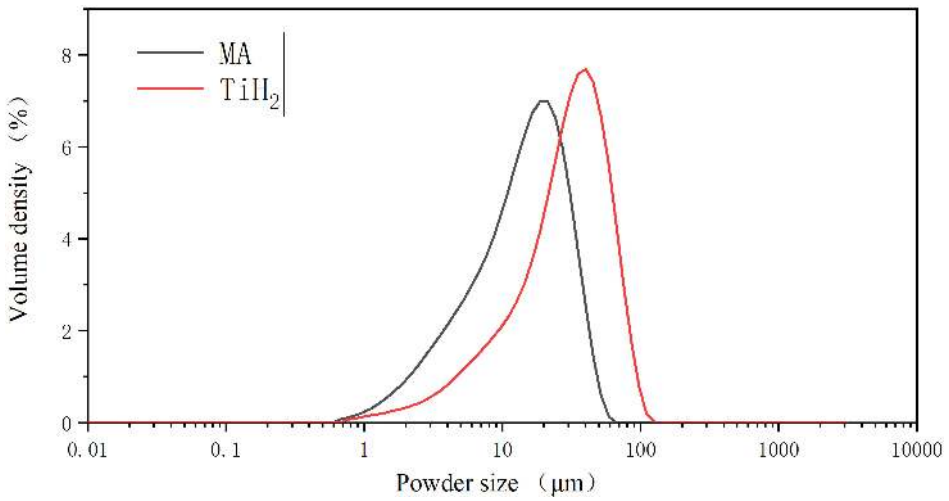

FIGURE 2 | Size distribution curve of TiH_2 and master alloy (MA) powders.

density level. After sintering, materials were cooled in the furnace down to room temperature.

To investigate the potential of post-sintering hot deformation for microstructure improvement, cylindrical green compacts of 29 mm in diameter and 140 mm long, which are suitable for hot deformation, were produced via Cold isostatic Pressing (CIP) under 300 MPa for 10 min. The CIP-treated powder blend preforms were vacuum sintered at 1200°C for 4 h, such sintering regime provides formation of uniform microstructure with minimized porosity. The as-sintered Ti80 billets were then treated by hot rolling in air at 950°C.

Characterization of Sintered Materials

Scanning electron microscopy (SEM, Vega 3 TESCAN) and optical microscopy (Leika Zeiss) were used to study the microstructures of the samples sintered following the above procedure. The Kroll reagent (3%HF, 6%HNO_3, 91%H_2O) was used to reveal the constituent microstructure for light microscopy. The density of the sintered materials was measured via Archimedes' technique and the residual porosity was determined via optical microscopy on the polished cross-sections of the sintered samples. The oxygen, nitrogen, and hydrogen contents in the sintered materials were measured using a LECO 836 system. The chemical composition of the produced alloy was determined by Xi'an Hantang Analysis & Test Co., Ltd. To evaluate the mechanical properties following the various sintering regimes, tensile testing was performed at room temperature using turned cylindrical samples with a gauge diameter of 5 mm, length of 25 mm.

RESULTS AND DISCUSSION

Chemical Composition of Sintered Ti80 Materials

Inductively coupled plasma (ICP) analysis of the sintered material revealed that its average chemical composition was

comparable with the proportions expected for the Ti80 alloy (**Table 2**).

The average oxygen (0.18–0.21 wt%), nitrogen (0.0085–0.023 wt%), and hydrogen (0.21–3.7 ppm) contents for the samples sintered with all the tested regimes were at admissible levels. Usually, a 0.15–0.2 wt% content of oxygen in titanium alloys is desirable, a higher value would lower the ductility, while insufficient oxygen content negatively affects the alloy strength. Residual atmospheric impurities (oxygen and nitrogen) present in the sintering chamber, even at relatively good vacuum conditions, are scavenged by titanium; hence, the content of these impurities has a tendency to slightly increase with increasing sintering time and temperature. The reverse trend for hydrogen cleaning of the powder compacts was realized during vacuum heating within the range of $300 - 600°C$ (Ivasishin et al., 2012), when the majority of hydrogen is emitted from the material. Then, hydrogen completely escapes from titanium if the vacuum heating cycle is sufficiently long. For the temperature, time, and vacuum conditions used in our experiments, the hydrogen content decreased to a sufficient level to avoid hydrogen embrittlement (usually, the standard requirements for hydrogen content in titanium alloys are < 0.01 wt%). Therefore, all the tested sintering regimes provided acceptable impurity (O, N, H) levels in the final samples, which is a necessary condition to achieve good mechanical properties.

Microstructure Analysis and Density Measurement

To select the optimized sintering regime and obtain superior material properties, a set of experiments was carried out to explore the relationship between the microstructure, density (i.e., residual porosity), and temperature-time condition.

To achieve a good balance of mechanical properties, the sintered material should demonstrate a completely uniform microstructure, minimized volume fraction of spherical residual pores, and a fine grain size. Usually, a longer duration at a higher sintering cycle temperature promotes chemical and microstructure uniformity of the material, a higher sintered density, and a desirable spherical morphology of residual pores, however, this simultaneously results in an increased grain size, which negatively affects the tensile elongation. Furthermore, insufficient sintering time and a low temperature results in a decrease in the relative density, inadequate time for pore healing, and potentially unfinished diffusion redistribution of the alloying elements in the titanium matrix, which results in considerable microstructure inhomogeneity. Such sintered microstructures are unsuitable because they naturally result in markedly poorer mechanical performance.

Taking into consideration the above points and the results of earlier studies dedicated to BEPM production of other titanium compositions (Ivasishin et al., 2008; Ivasishin and Moxson, 2015), we selected sintering temperatures in the range of $1100 - 1250°C$ which corresponds to the single-phase β field. At lower sintering temperatures α stabilizing aluminum is able to block diffusion redistribution of the β stabilizers (Nb, Mo) in the titanium matrix (Ivasishin et al., 2008) from the alloying particles, while temperatures $> 1250°C$ create a risk for excessive grain growth. The realization of chemical uniformity of the alloyed titanium matrix usually takes ∼2 h or more, and this is considerably dependent on the size and chemical composition of the alloying powder used as well as on temperature. Taking into consideration the relatively low diffusion mobility of Nb and Mo in titanium (Kale and Patil, 1994; Thibon et al., 1998; Laik et al., 2006), we tested sintering times of 3 and 4 h.

TABLE 2 | Chemical composition of sintered material (wt.%).

Al	Mo	Zr	Nb	Fe	Ti
5.78	0.97	1.83	2.94	0.23	balanced

The microstructures of the sintered materials are shown in **Figures 3a–e**. An important observed result is that all the used time-temperature sintering regimes realized sufficient microstructural uniformity; thus, the transformation of the heterogeneous powder blend into a homogeneous alloy was achieved. The as-sintered Ti80 materials demonstrated a typical lamellar $\alpha + \beta$ microstructure, which formed during cooling to room temperature after sintering within the β phase field. It should be noted that the α lamellae precipitated inside β grains were nearly the same size for all sintering regimes; this can be attributed to the same post-sintering cooling rate. An exception is the presence of some relatively coarse isolated α-phase crystallites of near equiaxed shape located among the lamellar $\alpha + \beta$ structure, which can be seen at the lowest sintering temperature of 1100°C (**Figures 3a,b**).

Coarse α-phase precipitates also clearly formed at some of the locations with increased concentration of α stabilizers (Al, as well as O and N impurities); this could either be attributed to remnants of the α phase that were not totally transformed into the β phase during sintering at 1100°C, or, more probably, they formed during cooling because of the higher rate of α nucleation and growth at these locations.

Time-temperature parameters of the sintering clearly affected the size of the β grains and the residual porosity. The relationship of the β grain size and the sintered density are shown in **Figures 4**, **5**. It can be observed from the corresponding microstructures (**Figure 3**) that grain growth increases alongside increasing sintering temperature, resulting in coarser β grains. Additionally, the grain size is naturally coarser for longer sintering times (sintering for 4 h compared with the 3 h group, **Figure 4**).

The density values markedly increased with temperature and time with a corresponding decrease in the residual porosity. The increased density demonstrated a non-linear behavior with temperature, with noticeable densification as the temperature increased from 1150 to 1200°C. Low sintering temperatures (1100 and 1150°C) led to the lowest density values for both 3 and 4 h sintering durations (**Figure 5**). From **Figure 3**, it can be seen that the sintering temperatures resulted in a wider size distribution of residual pores and their shape was far from spherical (**Figure 3a** as an example). The evolution of the pore structure on densification began with extensive healing of the pores during material heating and at the very beginning stages of

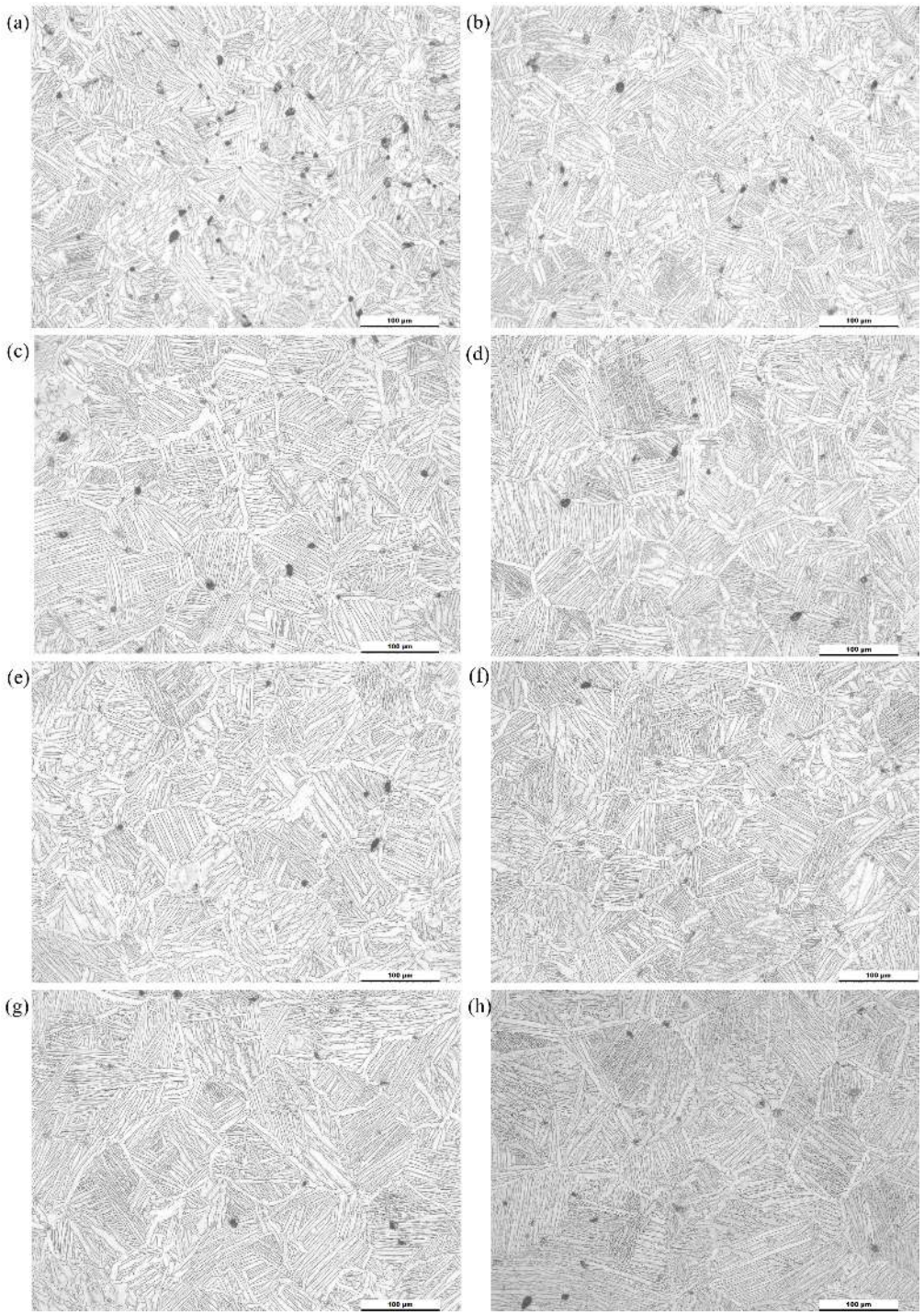

FIGURE 3 | Microstructure of sintered material: **(a,c,e,g)** represent 3 h at 1100, 1150, 1200, 1250°C; **(b,d,f,h)** represent 4 h at 1100, 1150, 1200, 1250°C, respectively.

isothermal sintering, then, this process slowed down. Because the pores are effective barriers for grain boundary movement, which restricts grain merging and growth, grain growth was minimal in these stages. A gradual decrease in the volume fraction of the pores with time led to more pronounced grain growth (**Figure 3b**), while densification slowed. There was minimal possibility for intragrain pores to be eliminated in the coarse grained structures via the vacancy flowing mechanism, which is because of the large distance from the pores to the nearest grain boundaries where vacancies annihilate. Hence, instead of

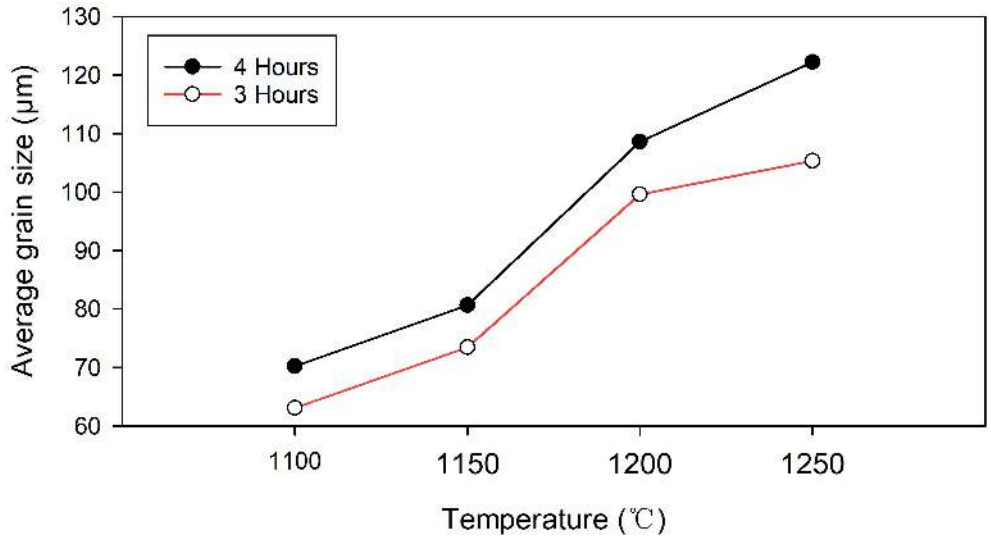

FIGURE 4 | The average β grain size depending on time-temperature sintering conditions.

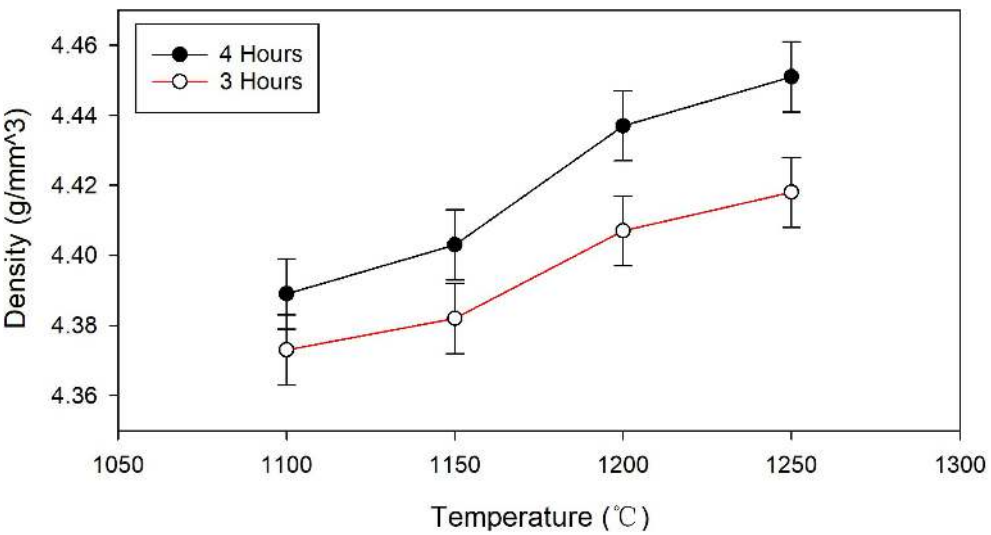

FIGURE 5 | Density of the Ti80 materials depending on sintering temperature and time.

pore healing, pore coalescence became more probable in the coarse-grained structures (small pores merged into a larger one inside the coarse grain).

Insufficient time and temperature have a noticeable impact on the pore healing process, which caused the difference in **Figure 3**. At relatively low temperatures (1100 − 1150°C) densification was hindered and remained far from realization of the full potential density, with preservation of the increased volume fraction of pores (2.7–3.1%, **Figures 3a,b**). The pores heal with increasing temperature and sintering time (**Figure 6**), while their shape gradually transformed from an irregular shape (**Figure 6A**) to a spherical one with increased sintering (**Figure 6B**). The lowest porosity measured was 1.3% for the regime at 1250°C for 4 h.

Irregular pore morphology (elongated with sharp corners) is detrimental to the mechanical properties. The locations with such pores become a weak area during loading and deformation. For achievement of high overall performance, residual pores with a spherical morphology and small size are preferable.

The non-linear dependence of the density growth (**Figure 5**) once more confirms the inability to achieve dense (poreless) structures with increased temperature and sintering time. The retardation of the densification process can be caused by gases trapped in the pores, while pore channels between the powder particles close. It should be noted that hydrogen emission from the titanium hydride powder and the emission of other volatile impurities usually takes place at relatively low temperatures (below ∼ 800°C) when the pore channels are not yet closed,

thus, eliminating the noted negative effect on densification in present case. However, lengthening the sintering time or rise temperature would not effectively help the density, otherwise it would result in noticeably larger beta grain size, which is undesirable in most cases.

Tensile Properties

The typical stress-strain behavior lines of the 4-h-sintered Ti80 materials are displayed in **Figure 7**. It can be seen that all the samples demonstrated an acceptable balance of strength and ductility. On increasing the sintering temperature from 1100 to 1250°C, the ultimate tensile strength and yield stress values increased. This behavior can be attributed mainly to the useful decrease in residual porosity with increased sintering temperature, while simultaneous increase in grain size as well as analog intragrain $\alpha + \beta$ microstructure and grain boundary α layers formed due to similar cooling conditions for all materials does not noticeably affect strength characteristics.

In more detail, the relationship of the ultimate tensile strength (UTS) and elongation of different Ti80 materials is shown in **Figure 8**. Both the tensile strength and ductility increased with increased sintering time, but a drop in tensile elongation is

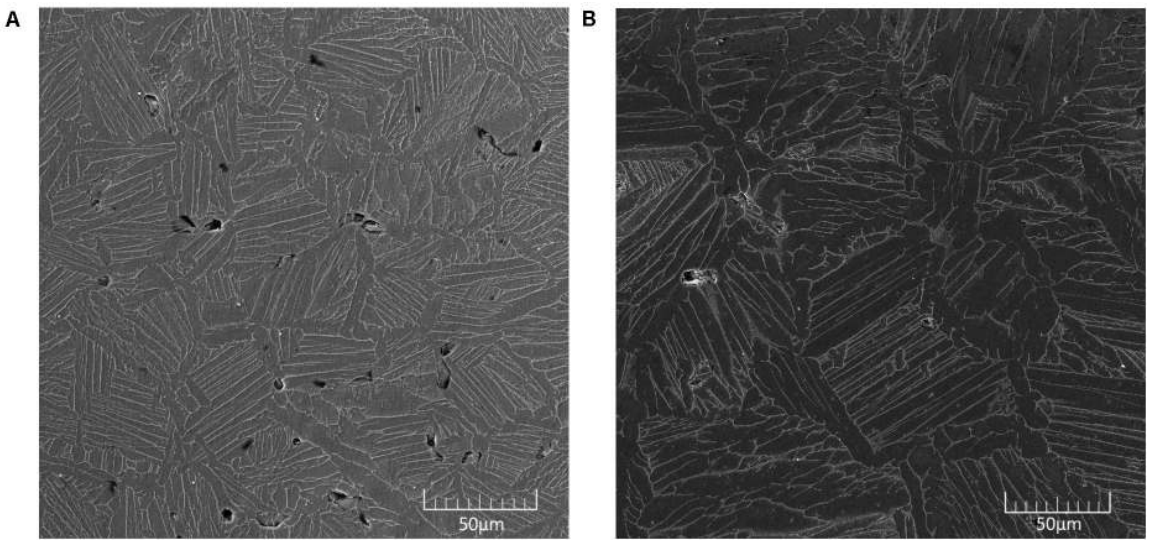

FIGURE 6 | Transformation of porosity in sintered Ti80 alloy depending on sintering temperature: **(A)** 1100°C 4 h and **(B)** 1250°C 4 h (SEM).

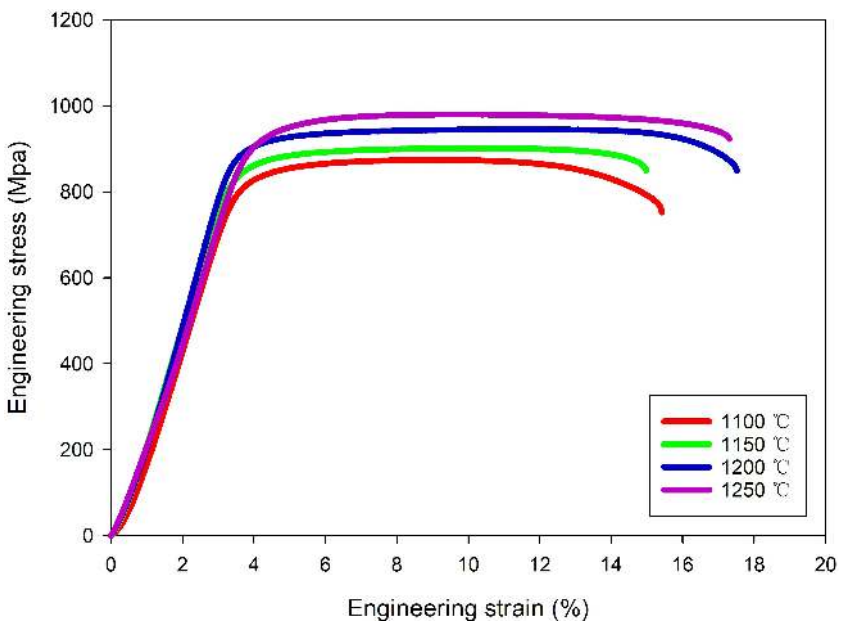

FIGURE 7 | Stress-Strain curves for the Ti80 samples sintered at different temperatures for 4 h.

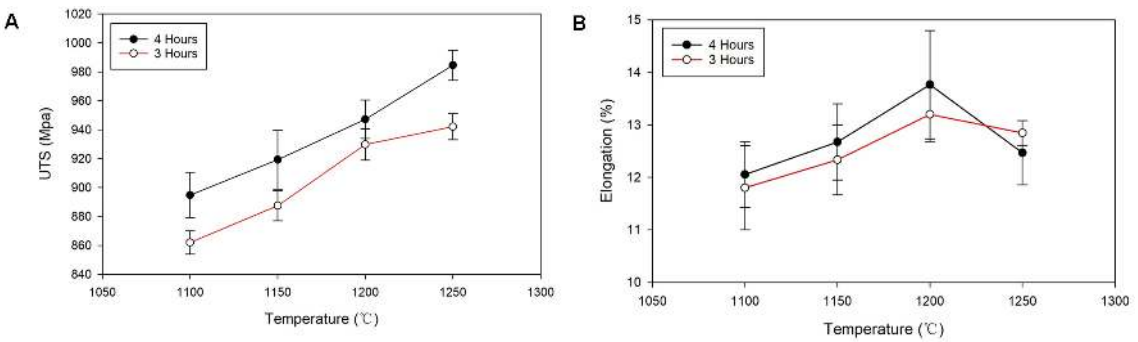

FIGURE 8 | UTS **(A)** and elongation **(B)** of sintered Ti80.

observed from 1200 to 1250°C. This can be explained by the simultaneous effect of the residual porosity and grain size on the mechanical characteristics (**Table 3**). A longer sintering time and higher temperature result in a decrease in residual porosity (from ∼3 to 1%) along with simultaneous β grain growth (from 63 to 122 μm). A lower porosity with fine residual pores and a spherical shape is preferable for both strength and elongation characteristics. However, the formation of coarse grains is detrimental for ductility, while having a negligible effect on strength. This is why the structure with minimized porosity demonstrated an effective improvement in the strength independently on coarse grains formation. The elongation demonstrated a similar trend as the temperature increased up to 1200°C; further increasing the temperature resulted in the reverse trend compared with the UTS. The ductility decreased for the highest sintering temperature of 1250°C; this is because the negative effect of the coarse (122 μm) grains was more significant than the positive contribution afforded by the reduced porosity. It should be noted, some difference in tensile characteristics for similar samples (error values noted in **Table 3**) with corresponding error bars shown in **Figure 8** can be explained mainly with random distribution of pores over the material. Non-uniformity in size, morphology and locations of residual pores slightly affects strength characteristics, while becomes more significant for tensile elongation.

It can be concluded that the optimal balance of tensile characteristics is realized with the microstructure obtained with sintering at 1200°C for 4 h, which gives an optimized grain size and reduced porosity. However, if specific conditions of practice application of produced Ti80 materials need highest possible strength without rigid requirements to ductile characteristics, the sintering temperature should be increased to 1250°C.

TABLE 3 | Room temperature tensile properties and microstructure characteristics of the Ti80 alloys.

	UTS (MPa)	Elongation (%)	Average residual porosity (%)	Average β grain size (μm)
1100°C-4 h	890 ± 15	12.2 ± 0.5	2.7%	70.2
1100°C-3 h	863 ± 17	11.9 ± 0.6	3.1%	63.1
1150°C-4 h	920 ± 20	12.7 ± 0.6	2.4%	80.75
1150°C-3 h	884 ± 14	12.1 ± 0.9	2.9%	73.7
1200°C-4 h	948 ± 12	14.0 ± 0.8	1.6%	108.6
1200°C-3 h	926 ± 14	13.2 ± 0.5	2.3%	99.6
1250°C-4 h	987 ± 8	12.4 ± 0.6	1.3%	122.2
1250°C-3 h	943 ± 8	12.7 ± 0.4	2.0%	105.3

Figure 9 shows an SEM images of the fracture surface with sintering at 1200 and 1100°C for 4 h after tensile testing at room temperature. Both (a) and (b) show a dimple fracture of the material; but (b) clearly shows a coarse surface and larger dimples than a), which indicated that the structure in (b) has inferior ductility.

Hot Deformation

To investigate the possibility of obtaining a modified poreless microstructure for the Ti80 alloy via post-sintering treatment, bars of CIP-treated samples at 300 MPa with sintering at 1200°C for 4 h were used. The as-sintered CIP TI80 shows an average density of $4.39 g/cm^3$, which is close to the value of $4.42\ g/cm^3$ obtained under the same sintering condition after uniaxial die compaction at 600 MPa. Sintered bars 26.5 ± 0.5 mm in diameter were hot rolled at 950°C, lower than phase transformation point (Yuan et al., 2013), with a diameter reduction to 15.5 ± 1 mm; thus, the reduction in the cross sectional area indicates ∼66% deformation occurred.

In **Figure 10**, the optical microscopy microstructure after rolling indicated that the lamellar α + β structure had been substantially broken and most of the pores were eliminated. Archimedes' technique revealed that the average density reached ∼4.49 g/cm^3, such an increase in density is in accordance with the less than 0.4% fine pore content observed in the microstructure (**Figure 10**). With the crushed structure, the grain boundaries could be hardly recognized, however, a refined basket weave structure with a relatively low residual porosity is promising for further improvement of the mechanical properties, such as the tensile strength, elongation, and fatigue characteristics. A reduction in the deformation temperature is a potential route to produce a poreless equiaxed microstructure. Thus, post-sintering hot deformation of Ti80 alloy can be recommended for some specific applications to meet rigid requirements for the mechanical characteristics.

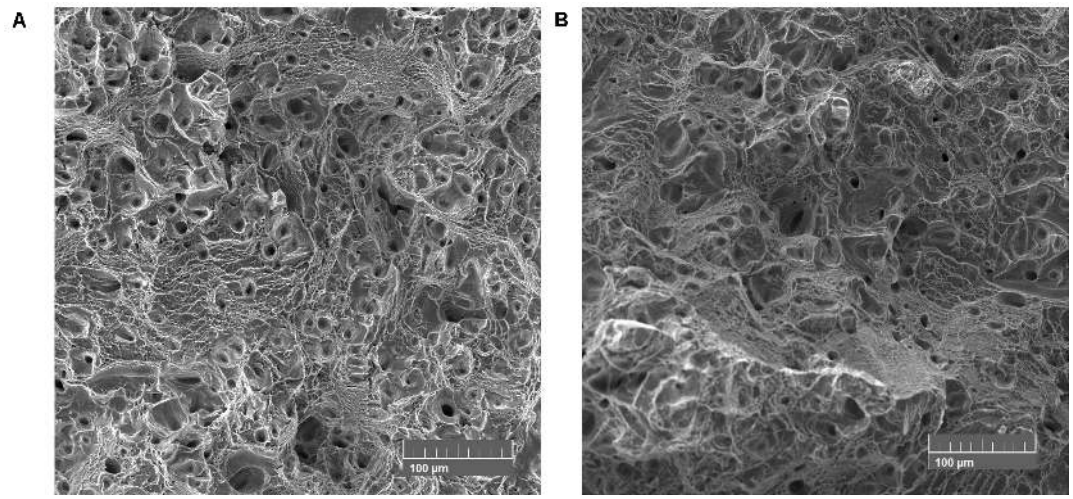

FIGURE 9 | Fracture surfaces of the Ti80 alloys produced with 4 h sintering at: **(A)** 1200°C and **(B)** 1100°C.

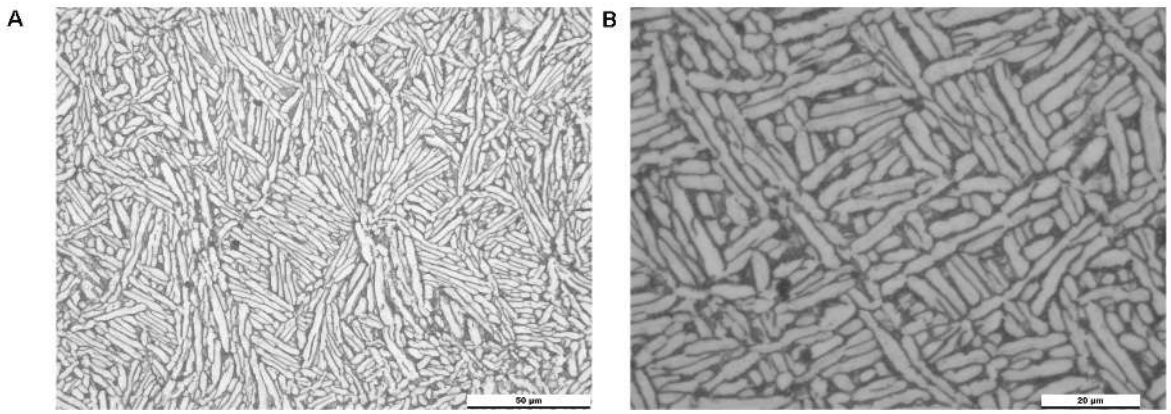

FIGURE 10 | As-rolled Ti80 microstructures via optical microscop at ×500 **(A)** and ×1000 **(B)** magnification.

CONCLUSION

1. In this work, a uniform low-porous Ti80 alloy with an acceptable impurity content was produced via the press-and-sinter BEPM approach using blends of TiH_2 and Al-Zr-Nb-Mo master alloy powders.
2. The influence of different time-temperature sintering parameters on the microstructure, including the residual porosity, grain size, and mechanical properties was carefully analyzed. The microstructure produced with sintering at 1200°C for 4 h shows the best balance of strength/ductility characteristics owing to the reduced residual porosity (1.6%) and relatively fine (108 μm) grain size.
3. The achieved balance of strength (UTS 948 ± 12 MPa) and ductile characteristics (elongation 14.0 ± 0.8%) is promising to consider practical application of the Ti80 alloy manufactured using the notably cost-effective BEPM approach.
4. Post-sintering hot deformation treatment, like rolling, can be recommended to form a dense Ti80 alloy (< 0.4% pores) with a refined α + β microstructure. Hot-deformed microstructures are promising for further improvement of mechanical characteristics.

DATA AVAILABILITY STATEMENT

All datasets presented in this study are included in the article/supplementary material.

AUTHOR CONTRIBUTIONS

BW collected the experimental data, performed the data analysis, and wrote the manuscript. PL and GM were involved in the work of rolling. DL, DS, and OI supervised the experiments and overall editing of the manuscript. All authors contributed to the article and approved the submitted version.

REFERENCES

Cao, F., Chandran, K. S. R., and Kumar, P. (2017). New approach to achieve high strength powder metallurgy Ti-6Al-4V alloy through accelerated sintering at β-transus temperature and hydrogenation-dehydrogenation treatment. *Scr. Mater.* 130, 22–26. doi: 10.1016/j.scriptamat.2016.11.005

Chen, G., Liss, K. D., Auchterlonie, G., Tang, H., and Cao, P. (2017). Dehydrogenation and sintering of TiH2: an in situ study. *Metall. Mater. Trans. A* 48, 2949–2959. doi: 10.1007/s11661-017-4043-8

Fang, Z. Z., Paramore, J. D., Sun, P., Chandran, K. S. R., Zhang, Y., Xia, Y., et al. (2017). Powder metallurgy of titanium – past, present, and future. *Int. Mater. Rev.* 63, 407–459. doi: 10.1080/09506608.2017.1366003

Fukai, Y. (2003). Formation of superabundant vacancies in M–H alloys and some of its consequences: a review. *J. Alloys Compd.* 356-357, 263–269. doi: 10.1016/s0925-8388(02)01269-0

Huang, Y., Tang, H., Jia, W., Liu, H., and He, W. (2011). Influence of element addition ways on the performance of Ti-6Al-3Nb-2Zr-1Mo Alloy. *Rare Metal Mater. Eng.* 40, 163–167.

Ivasishin, O. M., Anokhin, V. M., Demidik, A. N., and Savvakin, D. G. (2000). Cost-effective blended elemental powder metallurgy of titanium alloys for transportation application. *Key Eng. Mater.* 188, 55–62. doi: 10.4028/www.scientific.net/KEM.188.55

Ivasishin, O. M., Eylon, D., Bondarchuk, V. I., and Savvakin, D. G. (2008). Diffusion during powder metallurgy synthesis of titanium alloys. *Defect Diffus. Forum* 277, 177–185. doi: 10.4028/www.scientific.net/DDF.277.177

Ivasishin, O. M., and Moxson, V. S. (2015). Low-cost titanium hydride powder metallurgy. *Titanium Powder Metall.* 2015, 117–148. doi: 10.1016/b978-0-12-800054-0.00008-3

Ivasishin, O. M., Savvakin, D. G., Gumenyak, M. M., and Bondarchuk, O. B. (2012). Role of surface contamination in titanium PM. *Key Eng. Mater.* 520, 121–132. doi: 10.4028/www.scientific.net/KEM.520.121

Kale, G. B., and Patil, R. V. (1994). Chemical diffusion in titanium-molybdenum system. *Mater. Trans. Jim* 35, 439–444. doi: 10.2320/matertrans1989.35.439

Laik, A., Kale, G. B., and Bhanumurthy, K. (2006). Interdiffusion studies between a Mo-based alloy and Ti. *Metall. Mater. Trans. A* 37, 2919–2926. doi: 10.1007/s11661-006-0173-0

Liu, Y., Chen, L. F., Tang, H. P., Liu, C. T., Liu, B., and Huang, B. Y. (2006). Design of powder metallurgy titanium alloys and composites. *Mater. Sci. Eng. A* 418, 25–35.

Paramore, J. D., Fang, Z. Z., Dunstan, M., Sun, P., and Butler, B. G. (2017). Hydrogen-enabled microstructure and fatigue strength engineering of titanium alloys. *Sci. Rep.* 7:41444. doi: 10.1038/srep41444

Thibon, I., Ansel, D., Boliveau, M., and Debuigne, J. (1998). Interdiffusion in the β Mo - Ti Solid Solution at High Temperatures. *Zeitschrift Für Metallkunde* 89, 187–191.

Yuan, M., Cao, Y., Zhang, Y., Jiangtao, Y., Ji, L. I., and Zhang, L. (2013). Measurement for phase transformation Point of Ti80 Alloy. *Hot Work. Technol.* 42, 57–59. doi: 10.14158/j.cnki.1001-3814.2013.14.036

Conflict of Interest: The authors declare that the research was conducted in the absence of any commercial or financial relationships that could be construed as a potential conflict of interest.

The handling editor declared a past co-authorship with one of the authors OI.